BS 2023 4-6 SEPT SHANGHAI

International Building Performance Simulation Association

Optimal sensor/actuator placement and Control of Buildings Sub-zones to Spatio-temporal Profiles

Raman Goyal, Aayushman Sharma, Alejandro E Brito, Saman Mostafavi
Palo Alto Research Center (PARC), Palo Alto, California, USA

Abstract

We propose a novel framework to jointly optimize the placement of actuators and sensors, as well as the control laws for optimally controlling sub-zonal, spatiotemporal temperature profiles in a spacious room. Unlike traditional approaches focusing on simulation-assisted individual component design, our approach considers the inverse joint design problem, leading to a mathematically rigorous formulation. We employ a co-optimization framework based on Linear Matrix Inequalities (LMI) to distribute sensors and actuators throughout the system and achieve optimal precision while compensating for external disturbance and unmodeled dynamics using covariance control. Our approach enables building occupants to specify their preferences and evaluate the predicted performance of various configurations during the design phase, resulting in occupant-customized building control systems. Our preliminary results show that our approach effectively minimizes energy consumption while actively rejecting disturbances to achieve the desired spatiotemporal temperature profile in a subzonal environment. Overall, our work represents a significant step toward a more occupant-centric approach to designing building control systems.

Highlights

- Proposed a novel system design framework for energy-efficient building control systems that jointly optimizes the placement of actuators and sensors, as well as the control laws used to regulate them.
- Formulated the problem as an inverse joint design problem, leading to a mathematically rigorous framework based on Linear Matrix Inequalities (LMI) and robust feedback control.
- Developed a novel sensor/actuator selection algorithm to determine the optimum number of sensors/actuators needed for achieving the desired closed-loop control performance.
- Demonstrated the effectiveness of the proposed framework in minimizing energy consumption while actively rejecting disturbances to achieve the desired temperature profile.

Introduction

The importance of building control systems in achieving energy-efficient buildings cannot be overstated. While individual components such as sensors, actuators, and controllers have been extensively studied by researchers, the interaction between these components has received significantly less attention. Moreover, many buildings, such as commercial ones with large auditoriums and data centers, have non-uniform heat ventilation and heat generation, creating an opportunity for customized sub-zonal control. However, there are several challenges in addressing these issues. Many existing buildings lack advanced control systems, and some even lack HVAC or have poorly placed sensors. Additionally, some buildings lack actuation capabilities. Large spaces such as office buildings or concert halls may require multiple temperature zones but often lack adequate sensing and actuation requirements.

To overcome these challenges, researchers have proposed various model-based and data-driven approaches to determine the optimal number and location of sensors and actuators. These include controllability and observability gramians, mean square error minimization, and distributed parameter control theory. Furthermore, coupled simulations of HVAC control systems and envelope CFD models have been explored for simulation-assisted performance analysis (Zuo et al., 2016; Qiao et al., 2019). This review aims to provide a summary of recent advances in sensor and actuator placement to optimize building control systems.

Review of Placement Methods Optimal placement of sensors and actuators in building systems is a complex problem due to the nature of fluid flow physics, which is governed by coupled nonlinear partial differential equations subjected to disturbances, uncertainties, and complicated geometry (Vaidya et al., 2012). One approach utilizes controllability and observability gramians for actuator and sensor placement, respectively, in linear partial differential equations to control temperature or contaminants in a room (Vaidya et al., 2012). Another method minimizes the mean square error between estimated and correct temperature fields for optimal sensor placement, using the Kalman filter for temperature field estimation (Burns et al., 2012). A distributed parameter control theory-based approach has also been developed to opti-

https://doi.org/10.26868/25222708.2023.1423

mize sensor and actuator placement for maximizing observability and controllability (Borggaard et al., 2009).

Building energy systems employ sensor networks, such as temperature, humidity, illuminance, motion, and CO2 sensors, to monitor indoor environments and provide necessary information for intelligent control and management (Bae et al., 2021). Various optimization approaches have been explored, including data-driven techniques (Yoganathan et al., 2018), automatic sensor arrangement systems (Kim et al., 2012), and model-based optimization methods (Tran et al., 2019).

Other optimization techniques have been applied to determine the optimal placement of building system components. Particle swarm optimization was used to identify thermostat locations that optimize thermal comfort (Tian et al., 2018). Chen and Li (2016) developed virtual sensors by combining temperature statistics and Bayesian model fusion for spatial temperature distribution prediction. A simulation model and Sensor Optimization Unit (SOU) tool were developed to optimize temperature sensor placement in large sports spaces and reduce measurement uncertainty (Arnesano et al., 2016). A combinatorial optimization approach based on integer programming, using controllability and observability gramians for sensor and actuator placement, has also been proposed (Georges, 1995).

Recently, researchers have explored system design approaches where all components are cooperatively designed to achieve specified system performance (Li et al., 2008). Traditional practice involves designing individual components and modifying them for integration at the last step, often resulting in suboptimal solutions. The HVAC control design is typically separate from architectural and HVAC design, and controls are often not optimized after system construction. To address this, researchers have developed a computational framework for the co-design of control and sensor placement by simultaneously solving for control parameters and optimal sensor locations (Goyal and Skelton, 2019; Goyal et al., 2021a). This approach involves placing sensors at various possible locations and finding an optimal subset to maximize performance for a fixed number of sensors or to minimize the number of sensors required to obtain the desired performance.

Main Contribution In this paper, we present a complete integrated approach for designing occupant-customized building control systems, including control algorithms, personal comfort devices, and the location of wireless/BLE sensors. Our approach finds the balance between the observability and controllability of the system by optimizing the placement of personal comfort devices and sensors while also providing constraints on sensor/actuator placement (e.g., constraints on sensor locations to walls).

Our approach offers several benefits, including customized control to occupant preferences, minimized energy consumption, and improved temperature control in open office spaces. Additionally, our framework provides a retrofit solution for buildings without HVAC systems, improved system observability and controllability, and enhanced system robustness and disturbance rejection through robust feedback control. The ability to evaluate the predicted performance of various configurations during the design phase also results in a more efficient building control system.

Finally, our proposed approach has the potential for integration with smart home technologies and IoT systems for further energy savings and increased occupant convenience. We provide experimental results that demonstrate the effectiveness of our approach in achieving the desired temperature profile. Our work represents a significant step towards occupant-customized building control systems that consider the joint design problem of signal processing, personal comfort devices, and sensor location/precision selection.

Methodology

We consider the optimal placement and control of high Degree of Freedom (DoF) heat-diffusion Partial Differential Equations (PDEs). The methodology employs a cutting-edge, in-house sensor commissioning technology that allows for the placement and tracking of sensors using Augmented Reality (AR), streaming and querying data on-demand, and supplying relevant boundary conditions for a PDE model. This information is subsequently utilized in the modeling module, where sparse sensor data is interpolated onto a regular grid. The PDE model is discretized into a system of ordinary differential equations, and the data is employed to calibrate the linear system. This model is subsequently utilized by the placement and control module, where the sensor locations, actuator characteristics, and feedback control laws are co-optimized to yield an optimal control solution. In the following sections, we present the details of each module and provide a mathematically rigorous formulation for the optimal design framework.

Heat Diffusion Model Calibration with Experimental Data

This section outlines the linear dynamics model of 2D heat flow within a room and offers details on calibrating the PDE models using real sensor data obtained from the experimental test bed.

2D Heat Transfer PDE

The heat transfer equation, in its general form, can be expressed as:

$$\frac{\partial \theta(x,t)}{\partial t} = \nabla.(\alpha(\theta)\nabla\theta(x,t)) \tag{1}$$

where α represents the thermal diffusivity and $\theta = \theta(x,t)$ denotes the spatio-temporal temperature profile. In the context of control theory, θ serves as the system's state and is infinite-dimensional, signifying a spatio-temporally varying function.

https://doi.org/10.26868/25222708.2023.1423

Discretizion and calibration for PDE model

The phase field is discretized into a 2D grid of dimensions $N \times N$. Let $\theta_t^{i,j}$ represent the phase field of the cell defined by grid location (i, j) for all $i, j = 1, ..., N$, at time t. Employing a central-difference scheme based on eq. (1), we obtain the high-dimensional 2D phase-field model. Rearranging the terms yields the time-variation of the local phase field:

$$\theta_{t+1}^{i,j} = \theta_t^{i,j} + \alpha \Delta t \left(\frac{\theta_t^{i+1,j} + \theta_t^{i-1,j} + \theta_t^{i,j+1} + \theta_t^{i,j-1} - 4\theta_t^{i,j}}{\Delta x^2} \right) \tag{2}$$

with the boundary conditions $\theta_t^{i,N} = T_{right-wall}(t)$, $\theta_t^{i,0} = T_{left-wall}(t)$, $\theta_t^{0,j} = T_{upper-wall}(t)$ and $\theta_t^{N,j} = T_{lower-wall}(t)$. Only considering the diffusion term, eq. (2) can be written in the following discrete state-space representation:

$$\theta_{t+1} = A\theta_t \tag{3}$$

For calibration, we employ the following least square scheme:

$$\min_A \sum_{i=1}^{n} \left\| \hat{y}_t^{i,j} - A\theta_t^{i,j} \right\|^2 \tag{4}$$

That is, minimization of the sum of squared differences between the interpolated outputs $\hat{y}_t^{i,j}$ and the model predictions[1].

Given the temperature profile vector θ_t and the control input vector u_t at any time t, formed as a stack of all states $\{\theta_t^{i,j}\}$ and control inputs $\{u_t^{i,j}\} = \{T_t^{i,j}\}^T$, respectively, we can simulate the phase-field at the next time step from eq. (2).

The Linear State Space Representation

The given system of equations can be expressed as a linear time-varying system in discrete-time using state space representation as follows:

$$\theta_{t+1} = A\theta_t + Bu_t + Dw_t + Ew_t^a, \text{ (State)} \tag{5}$$
$$\theta_t^s = C\theta_t + Fw_t^s, \text{ (Measurement)} \tag{6}$$
$$\theta_t^z = C_z\theta_t, \text{ (Desired Output)} \tag{7}$$

for $t = \{0, 1, \cdots, N\}$ and where $\theta_t \in \mathbb{R}^n$ is the state of the system at time-step t, $u_t \in \mathbb{R}^m$ is the control vector, $\theta_t^s \in \mathbb{R}^p$ is the measurement of the system. The noise in the system is added through process noise w_t, actuator noise w_t^a, and sensor noise w_t^s. These noisy inputs to the system are modeled as independent zero mean white noises with covariances $\mathbb{W} \succ 0$, $\mathbb{W}^a \succ 0$ and $\mathbb{W}^s \succ 0$, respectively. We assume the process noise covariance $\mathbb{W}$ to be known and fixed. The precision of the actuators and sensors is defined as the inverse of the variance of the actuator noise and sensor noise that are independent of each other.

$$\mathbf{\Gamma}^a \triangleq \mathbf{diag}(\gamma_a) \triangleq \mathbb{W}^{a^{-1}}, \quad \mathbf{\Gamma}^s \triangleq \mathbf{diag}(\gamma_s) \triangleq \mathbb{W}^{s^{-1}}.$$

[1]The authors have submitted a paper explaining their data collection method and PDE calibration in detail. To comply with the double-blind review process, we have removed this information from the submission currently under review and plan to add it back upon acceptance.

Similar to Li et al. (2008), we assign a price to each actuator/sensor, which is inversely proportional to the noise intensity of that instrument. Thus, the overall design price can be formulated as:

$$\$ = p_a^T \gamma_a + p_s^T \gamma_s,$$

where p_a and p_s are vectors containing the price per unit of actuator precision and sensor precision, respectively.

Notice that the system dynamics eq. (5) can be written as:

$$\theta_{t+1} = A^{t+1}\theta_0 + \boldsymbol{B}_t U_t + \boldsymbol{D}_t W_t + \boldsymbol{E}_t W_t^a, \tag{8}$$

where the vectors U_t, W_t and W_t^a are defined as:

$$U_t = \begin{bmatrix} u_0 \\ u_1 \\ \vdots \\ u_t \end{bmatrix}, \; W_t = \begin{bmatrix} w_0 \\ w_1 \\ \vdots \\ w_t \end{bmatrix}, \; W_t^a = \begin{bmatrix} w_0^a \\ w_1^a \\ \vdots \\ w_t^a \end{bmatrix}, \tag{9}$$

and matrices $\boldsymbol{B}_t$, $\boldsymbol{D}_t$ and $\boldsymbol{E}_t$ are defined as:

$$\boldsymbol{B}_t = \begin{bmatrix} A^t B & A^{t-1}B & \cdots & B \end{bmatrix}, \tag{10}$$
$$\boldsymbol{D}_t = \begin{bmatrix} A^t D & A^{t-1}D & \cdots & D \end{bmatrix}, \tag{11}$$
$$\boldsymbol{E}_t = \begin{bmatrix} A^t E & A^{t-1}E & \cdots & E \end{bmatrix}. \tag{12}$$

Similarly, the state and measurement equation in augmented vector form can be written as:

$$\Theta_{t+1} = \bar{\mathbf{A}}_t \theta_0 + \bar{\mathbf{B}}_t U_t + \bar{\mathbf{D}}_t W_t + \bar{\mathbf{E}}_t W_t^a, \tag{13}$$
$$\Theta^s = \bar{\mathbf{C}}_t \Theta_t + \bar{\mathbf{F}}_t W_t^s, \tag{14}$$

where

$$\Theta_{t+1} = \begin{bmatrix} \theta_0 \\ \theta_1 \\ \vdots \\ \theta_{t+1} \end{bmatrix}, \; \Theta_t^s = \begin{bmatrix} \theta_0^s \\ \theta_1^s \\ \vdots \\ \theta_t^s \end{bmatrix}, \; W_t^s = \begin{bmatrix} w_0^s \\ w_1^s \\ \vdots \\ w_t^s \end{bmatrix}, \tag{15}$$

and the augmented system matrices $\bar{\mathbf{A}}_t, \bar{\mathbf{B}}_t, \bar{\mathbf{D}}_t, \bar{\mathbf{E}}_t, \bar{\mathbf{C}}_t, \bar{\mathbf{F}}_t$ can be written accordingly. Finally, the augmented measurement equation can be written as:

$$\Theta^s = \bar{\mathbf{C}}_t \bar{\mathbf{A}}_{t-1} \theta_0 + \bar{\mathbf{C}}_t \bar{\mathbf{B}}_{t-1} U_{t-1} + \bar{\mathbf{C}}_t \bar{\mathbf{D}}_{t-1} W_{t-1} + \bar{\mathbf{C}}_t \bar{\mathbf{E}}_{t-1} W_{t-1}^a + \bar{\mathbf{F}}_t W_t^s. \tag{16}$$

Optimal Placement and Control of Building Sub-zones

Problem Statement

The placement approach is depicted in Figure 1. We choose an affine control law of the following form (similar to Goyal et al. (2021b)):

$$U_t = V_t + \bar{\boldsymbol{K}}_t (\Theta^s - \bar{\mathbf{C}}_t \bar{\mathbf{A}}_{t-1} \bar{\theta}_0 - \bar{\mathbf{C}}_t \bar{\mathbf{B}}_{t-1} U_{t-1}),$$

where V_t is the feedforward control vector and $\bar{\boldsymbol{K}}_t$ is the left lower triangular matrix representing the feedback gain

https://doi.org/10.26868/25222708.2023.1423

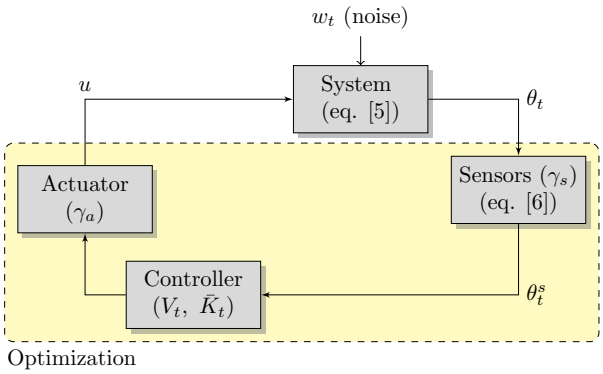

Figure 1: Diagram describing the overall placement approach.

matrix. The lower triangular structure makes sure that only past measurement and control information is used for the next control input. The final problem statement is to find the control law (V_N, $\bar{\boldsymbol{K}}_N$) and simultaneously select the appropriate actuator and sensor precisions such that:

$$\mathbb{E}[\theta^z_{N+1}] = \bar{\theta}^z_{N+1}, \;\; \mathbb{E}[\tilde{\theta}^z_{N+1}\tilde{\theta}^{z^T}_{N+1}] \preceq \boldsymbol{\Sigma}^z_{N+1}, \tag{17}$$

while minimizing the cost function J:

$$J = \mathbb{E}\left[\sum_{t=0}^{N}\left((\theta^z_t - \bar{\theta}^z_{N+1})^T \boldsymbol{Q}_t(\theta^z_t - \bar{\theta}^z_{N+1}) + u_t^T \boldsymbol{R}_t u_t\right)\right],$$

with the budget and precisions constraints as:

$$\$ < \bar{\$}, \;\; \gamma_a < \bar{\gamma}_a, \;\; \gamma_s < \bar{\gamma}_s, \tag{18}$$

for given $\bar{\$} > 0$, $\bar{\gamma}_a > \boldsymbol{O}$, $\bar{\theta}_0$, $\bar{\theta}^z_{N+1}$, and $\boldsymbol{\Sigma}^z_{N+1} \succeq 0$. The bounds on precision values can be added based on the most precise sensor available in the market.

Solution to the Problem Statement

Let us again write the control law using eq. (16) as:

$$\begin{aligned} U_t = V_t &+ \bar{\boldsymbol{K}}_t\left(\bar{\mathbf{C}}_t\bar{\mathbf{A}}_{t-1}(\theta_0 - \bar{\theta}_0)\right) \\ &+ \bar{\boldsymbol{K}}_t\left(\bar{\mathbf{C}}_t\bar{\mathbf{D}}_{t-1}W_{t-1} + \bar{\mathbf{C}}_t\bar{\mathbf{E}}_{t-1}W^a_{t-1} + \bar{\mathbf{F}}_t W^s_t\right), \end{aligned}$$

which can be written in a slightly different form by defining $\bar{\mathbf{K}}_t = [\bar{\boldsymbol{K}}_t \; \boldsymbol{O}]$ as:

$$\begin{aligned} U_t = V_t &+ \bar{\mathbf{K}}_t\left(\bar{\mathbf{C}}_{t+1}\bar{\mathbf{A}}_t(\theta_0 - \bar{\theta}_0)\right) \\ &+ \bar{\mathbf{K}}_t\left(\bar{\mathbf{C}}_{t+1}\bar{\mathbf{D}}_t W_t + \bar{\mathbf{C}}_{t+1}\bar{\mathbf{E}}_t W^a_t + \bar{\mathbf{F}}_{t+1}W^s_{t+1}\right). \end{aligned}$$

Using the above-mentioned control, we can write the state equation (eq. (13)) as:

$$\begin{aligned} \Theta_{t+1} = \bar{\mathbf{A}}_t\theta_0 + \bar{\mathbf{B}}_t V_t + \bar{\mathbf{D}}_t W_t + \bar{\mathbf{E}}_t W^a_t \\ + \bar{\mathbf{B}}_t\bar{\mathbf{K}}_t\bar{\mathbf{C}}_{t+1}\left(\bar{\mathbf{A}}_t(\theta_0 - \bar{\theta}_0) + \bar{\mathbf{D}}_t W_t + \bar{\mathbf{E}}_t W^a_t\right) \\ + \bar{\mathbf{B}}_t\bar{\mathbf{K}}_t\bar{\mathbf{F}}_{t+1}W^s_{t+1}. \end{aligned}$$

Taking the expectation of the above equation, the mean at the final time for considered output can be written as:

$$\bar{\theta}^z_{N+1} = C_z\bar{\mathbf{I}}_N\bar{\Theta}_{N+1} = C_z\bar{\mathbf{I}}_N(\bar{\mathbf{A}}_N\bar{\theta}_0 + \bar{\mathbf{B}}_N V_N), \tag{19}$$

where $\bar{\mathbf{I}}_N = \begin{bmatrix}\boldsymbol{O} & \cdots & \boldsymbol{O} & \boldsymbol{I}_n\end{bmatrix}$. The deviation from the mean, $\tilde{\Theta}_{t+1} = \Theta_{t+1} - \bar{\Theta}_{t+1}$, is written as:

$$\begin{aligned} \tilde{\Theta}_{t+1} = \left(I + \bar{\mathbf{B}}_t\bar{\mathbf{K}}_t\bar{\mathbf{C}}_{t+1}\right)\left(\bar{\mathbf{A}}_t\tilde{\theta}_0 + \bar{\mathbf{D}}_t W_t + \bar{\mathbf{E}}_t W^a_t\right) \\ + \bar{\mathbf{B}}_t\bar{\mathbf{K}}_t\bar{\mathbf{F}}_{t+1}W^s_{t+1}, \end{aligned}$$

and the covariance can be written as:

$$\begin{aligned} \mathbb{E}[\tilde{\Theta}_{t+1}\tilde{\Theta}^T_{t+1}] &= \bar{\mathbf{B}}_t\bar{\mathbf{K}}_t\bar{\mathbf{F}}_{t+1}\mathbb{W}^s_{t+1}(\bar{\mathbf{B}}_t\bar{\mathbf{K}}_t\bar{\mathbf{F}}_{t+1})^T \\ &+ \left(I + \bar{\mathbf{B}}_t\bar{\mathbf{K}}_t\bar{\mathbf{C}}_{t+1}\right)\left(\bar{\mathbf{A}}_t\boldsymbol{\Sigma}_0\bar{\mathbf{A}}^T_t\right)\left(I + \bar{\mathbf{B}}_t\bar{\mathbf{K}}_t\bar{\mathbf{C}}_{t+1}\right)^T \\ &+ \left(I + \bar{\mathbf{B}}_t\bar{\mathbf{K}}_t\bar{\mathbf{C}}_{t+1}\right)\left(\bar{\mathbf{D}}_t\mathbb{W}_t\bar{\mathbf{D}}^T_t\right)\left(I + \bar{\mathbf{B}}_t\bar{\mathbf{K}}_t\bar{\mathbf{C}}_{t+1}\right)^T \\ &+ \left(I + \bar{\mathbf{B}}_t\bar{\mathbf{K}}_t\bar{\mathbf{C}}_{t+1}\right)\left(\bar{\mathbf{E}}_t\mathbb{W}^a_t\bar{\mathbf{E}}^T_t\right)\left(I + \bar{\mathbf{B}}_t\bar{\mathbf{K}}_t\bar{\mathbf{C}}_{t+1}\right)^T, \end{aligned}$$

and the covariance at the final time for some desired output covariance constraint can be written as:

$$\mathbb{E}[\tilde{\theta}^z_{N+1}\tilde{\theta}^{z^T}_{N+1}] = C_z\bar{\mathbf{I}}_N\mathbb{E}[\tilde{\Theta}_{N+1}\tilde{\Theta}^T_{N+1}]\bar{\mathbf{I}}^T_N C^T_z \preceq \boldsymbol{\Sigma}^z_{N+1},$$

which further can be written as a linear matrix inequality using Schur's complement:

$$\begin{bmatrix} \boldsymbol{\Sigma}^z_{N+1} & C_z\bar{\mathbf{I}}_N\bar{\mathbf{G}}_1 & C_z\bar{\mathbf{I}}_N\bar{\mathbf{G}}_2 & C_z\bar{\mathbf{I}}_N\bar{\mathbf{G}}_3 & C_z\bar{\mathbf{I}}_N\bar{\mathbf{G}}_4 \\ (\bullet) & \boldsymbol{\Sigma}^{-1}_0 & \boldsymbol{O} & \boldsymbol{O} & \boldsymbol{O} \\ (\bullet) & (\bullet) & \mathbb{W}^{-1}_N & \boldsymbol{O} & \boldsymbol{O} \\ (\bullet) & (\bullet) & (\bullet) & \boldsymbol{\Gamma}^a_N & \boldsymbol{O} \\ (\bullet) & (\bullet) & (\bullet) & (\bullet) & \boldsymbol{\Gamma}^s_N \end{bmatrix} \succeq \boldsymbol{O},$$

where $\boldsymbol{\Gamma}^a_N = \boldsymbol{I}_N \otimes \boldsymbol{\Gamma}^a$, $\boldsymbol{\Gamma}^s_N = \boldsymbol{I}_N \otimes \boldsymbol{\Gamma}^s$ and $\bar{\mathbf{G}}_1 = (I + \bar{\mathbf{B}}_N\bar{\mathbf{K}}_N\bar{\mathbf{C}}_{N+1})\bar{\mathbf{A}}_N$, $\bar{\mathbf{G}}_2 = (I + \bar{\mathbf{B}}_N\bar{\mathbf{K}}_N\bar{\mathbf{C}}_{N+1})\bar{\mathbf{D}}_N$, $\bar{\mathbf{G}}_3 = (I + \bar{\mathbf{B}}_N\bar{\mathbf{K}}_N\bar{\mathbf{C}}_{N+1})\bar{\mathbf{E}}_N$, $\bar{\mathbf{G}}_4 = \bar{\mathbf{B}}_N\bar{\mathbf{K}}_N\bar{\mathbf{F}}_{N+1}$.

Now, the cost function can be written as:

$$J = \mathbb{E}[(\Theta_N - \bar{\mu}_{N+1})^T\bar{\boldsymbol{Q}}(\Theta_N - \bar{\mu}_{N+1}) + U^T_N\bar{\boldsymbol{R}}U_N],$$

where $\bar{\boldsymbol{Q}} = \boldsymbol{I}_N \otimes C^T_z\boldsymbol{Q}C_z$, $\bar{\boldsymbol{R}} = \boldsymbol{I}_N \otimes \boldsymbol{R}$, and $\bar{\mu}_{N+1} = \mathbf{1}_N \otimes \bar{\theta}_{N+1}$. The cost function is again written as:

$$\begin{aligned} J = (\bar{\Theta}_N - \bar{\mu}_{N+1})^T\bar{\boldsymbol{Q}}(\bar{\Theta}_N - \bar{\mu}_{N+1}) + \mathbb{E}[\tilde{\Theta}^T_N\bar{\boldsymbol{Q}}\tilde{\Theta}_N] \\ + V^T_N\bar{\boldsymbol{R}}V_N + \mathbb{E}[\tilde{U}^T_N\bar{\boldsymbol{R}}\tilde{U}_N], \end{aligned} \tag{20}$$

and after combining the terms and using the properties of the trace operator, we can write:

$$\begin{aligned} J = \mathrm{Tr}(\bar{\boldsymbol{Q}}(\bar{\Theta}_N - \bar{\mu}_{N+1})(\bar{\Theta}_N - \bar{\mu}_{N+1})^T + \bar{\boldsymbol{Q}}\mathbb{E}[\tilde{\Theta}_N\tilde{\Theta}^T_N]) \\ + \mathrm{Tr}(\bar{\boldsymbol{R}}V_N V^T_N + \bar{\boldsymbol{R}}\mathbb{E}[\tilde{U}_N\tilde{U}^T_N]), \end{aligned} \tag{21}$$

where $\mathrm{Tr}(\cdot)$ is the trace operator. Let us write the final cost minimization as:

$$\min.\left(\mathrm{Tr}(\boldsymbol{J}_x) + \mathrm{Tr}(\boldsymbol{J}_u)\right), \tag{22}$$

where we add the constraints on dummy variables J_x and J_u as:

$$\begin{aligned} \boldsymbol{J}_x \succeq \bar{\boldsymbol{Q}}^{1/2}(\bar{\Theta}_N - \bar{\mu}_{N+1})(\bar{\Theta}_N - \bar{\mu}_{N+1})^T\bar{\boldsymbol{Q}}^{1/2} \\ + \bar{\boldsymbol{Q}}^{1/2}\mathbb{E}[\tilde{\Theta}_N\tilde{\Theta}^T_N]\bar{\boldsymbol{Q}}^{1/2}, \end{aligned} \tag{23}$$

$$\boldsymbol{J}_u \succeq \bar{\boldsymbol{R}}^{1/2} V_N V_N^T \bar{\boldsymbol{R}}^{1/2} + \bar{\boldsymbol{R}}^{1/2} \mathbb{E}[\tilde{U}_N \tilde{U}_N^T] \bar{\boldsymbol{R}}^{1/2}. \quad (24)$$

The above matrix inequalities can finally be written as linear matrix inequalities using Schur's complement:

$$\begin{bmatrix} \boldsymbol{J}_x & (\star) & \bar{\boldsymbol{Q}}^{\frac{1}{2}} \bar{\mathbf{G}}_1 & \bar{\boldsymbol{Q}}^{\frac{1}{2}} \bar{\mathbf{G}}_2 & \bar{\boldsymbol{Q}}^{\frac{1}{2}} \bar{\mathbf{G}}_3 & \bar{\boldsymbol{Q}}^{\frac{1}{2}} \bar{\mathbf{G}}_4 \\ (\bullet) & \boldsymbol{I} & \boldsymbol{O} & \boldsymbol{O} & \boldsymbol{O} & \boldsymbol{O} \\ (\bullet) & (\bullet) & \boldsymbol{\Sigma}_0^{-1} & \boldsymbol{O} & \boldsymbol{O} & \boldsymbol{O} \\ (\bullet) & (\bullet) & (\bullet) & \mathbb{W}_N^{-1} & \boldsymbol{O} & \boldsymbol{O} \\ (\bullet) & (\bullet) & (\bullet) & (\bullet) & \boldsymbol{\Gamma}_N^a & \boldsymbol{O} \\ (\bullet) & (\bullet) & (\bullet) & (\bullet) & (\bullet) & \boldsymbol{\Gamma}_N^s \end{bmatrix} \succeq \boldsymbol{O},$$

where $(\star) = \bar{\boldsymbol{Q}}^{\frac{1}{2}} (\bar{\mathbf{A}}_N \bar{\theta}_0 + \bar{\mathbf{B}}_N V_N - \bar{\mu}_{N+1})$,

$$\begin{bmatrix} \boldsymbol{J}_u & \bar{\boldsymbol{R}}^{\frac{1}{2}} V_N & \bar{\boldsymbol{R}}^{\frac{1}{2}} \boldsymbol{\mathcal{H}}_1 & \bar{\boldsymbol{R}}^{\frac{1}{2}} \boldsymbol{\mathcal{H}}_2 & \bar{\boldsymbol{R}}^{\frac{1}{2}} \boldsymbol{\mathcal{H}}_3 & \bar{\boldsymbol{R}}^{\frac{1}{2}} \boldsymbol{\mathcal{H}}_4 \\ (\bullet) & \boldsymbol{I} & \boldsymbol{O} & \boldsymbol{O} & \boldsymbol{O} & \boldsymbol{O} \\ (\bullet) & (\bullet) & \boldsymbol{\Sigma}_0^{-1} & \boldsymbol{O} & \boldsymbol{O} & \boldsymbol{O} \\ (\bullet) & (\bullet) & (\bullet) & \mathbb{W}_N^{-1} & \boldsymbol{O} & \boldsymbol{O} \\ (\bullet) & (\bullet) & (\bullet) & (\bullet) & \boldsymbol{\Gamma}_N^a & \boldsymbol{O} \\ (\bullet) & (\bullet) & (\bullet) & (\bullet) & (\bullet) & \boldsymbol{\Gamma}_N^s \end{bmatrix} \succeq \boldsymbol{O},$$

where $\boldsymbol{\mathcal{H}}_1 = \bar{\mathbf{K}}_N \bar{\mathbf{C}}_{N+1} \bar{\mathbf{A}}_N$, $\boldsymbol{\mathcal{H}}_2 = \bar{\mathbf{K}}_N \bar{\mathbf{C}}_{N+1} \bar{\mathbf{D}}_N$, $\boldsymbol{\mathcal{H}}_3 = \bar{\mathbf{K}}_N \bar{\mathbf{C}}_{N+1} \bar{\mathbf{E}}_N$, $\boldsymbol{\mathcal{H}}_4 = \bar{\mathbf{K}}_N \bar{\mathbf{F}}_{N+1}$.

Simulation Results

In this section, we present the results obtained from applying our novel framework to a simulation case study. To obtain a more realistic scenario, we first gather data using in-house developed BLE sensors in a lab experiment. We then calibrate a diffusion heat transfer PDE model using the obtained data. Subsequently, we perform sensor/actuator placement for a few scenarios using the calibrated PDE model. We assume that heaters (heat sources) are used to create a temperature gradient profile. Although there is constant heat exchange between the air particles in a room but a mean temperature profile with some small variation can still be maintained using external heat sources in different regions of the room.

As mentioned earlier, the precision value of the actuators and sensors is the inverse of the variance of the respective noises, i.e., a small precision value means a sensor/actuator with high noise variance and thus a precision value of zero means the sensor/actuator with infinite noise. If the desired temperature profile can be obtained using a sensor with infinite noise (zero precision), then that particular sensor has no importance. Thus, the precision value of a sensor/actuator describes the importance of it relative to the other sensors/actuators. The units of the sensor/actuator precision values are $({}^oC^{-2})$.

Data acquisition and calibration of the discretized PDE model

Using our in-house developed BLE sensors, we conducted a lab experiment to collect temperature data under various conditions. The collected data served as the basis for calibrating our diffusion heat transfer PDE model, ensuring an accurate representation of the building's thermal behavior.

Placement in a meeting room

Figure 2 illustrates the initial profiles for an office used to hold meetings. The room was modeled as a 10/12 ft by 16 ft rectangle, divided into uniform grids of 4 square feet in size. We make the following assumptions in this simulation case study:

- Occupants of the room have different temperature preferences.
- The table in the middle of the room has corners with varying thermal conditions, reflecting the occupant's preferences.
- The budget is limited and sensor/actuator costs should be minimized.
- Actuation corresponds to heating, and initially, the room is kept at a lower temperature to save energy.

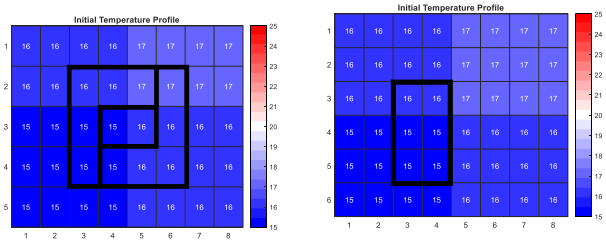

Figure 2: (Left) The assumed initial heat profile for the 5X8 grid configuration. (Right) The assumed initial heat profile for the 6X8 grid configuration.

Figure 3 displays the results for the joint placement and control of the heat profile, given the initial heat profile shown in Figure 2 (Left), and for the case when both sensors and actuators can be placed on each grid. Figure 3 (left) successfully demonstrate control of the grid points along the boundary of the table, achieving the desired temperature profiles of 22 and 24 ^oC. Figures 3 (middle) and (right) show the results for the actuator and sensor precision, respectively. The results reveal higher actuator precision requirements for the grid points over the table in order to precisely control the temperature at those points. Additionally, higher sensor precision requirements are observed for the neighboring grid points.

Final Placement of Actuators and Sensors

It is important to note that the precision results are guided by the optimization formulation presented in the paper's methodology section. As described in eq. (8), the overall design price, determined by the sum of the costs for actuator and sensor precision, aims to balance the trade-off between achieving accurate temperature control and minimizing the overall design cost. Without this optimization formulation, the results would trivially point to infinite precision in all grid points, which is not a practical or cost-effective solution. Next, we investigate two additional scenarios: one where the sensor and actuator locations are constrained, and another that focuses on an asymmetric case study.

Constraining actuators/sensors along the wall

Figure 4 presents the results when sensors and actuators can only be placed along the wall, effectively setting the precision for all other grid points to zero. Figure 4(left) demonstrates successful control of the bound-

https://doi.org/10.26868/25222708.2023.1423

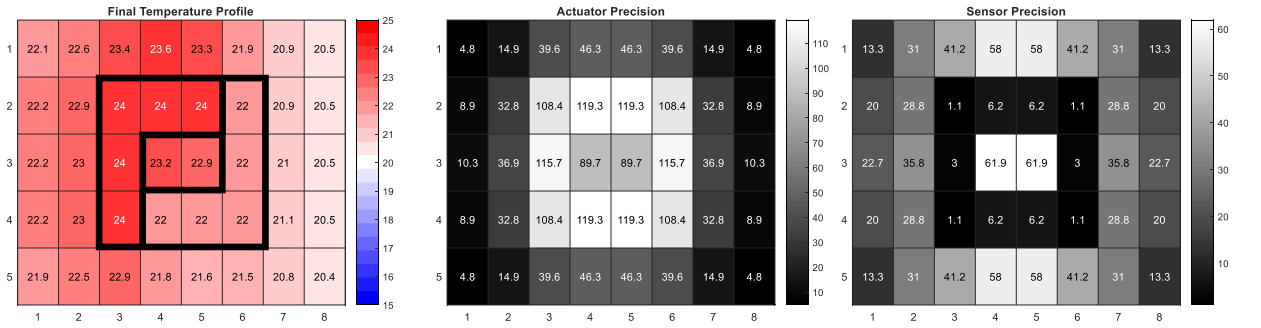

Figure 3: The final heat profile, actuator precision, and sensor precision values obtained using the developed design framework when actuators and sensors were placed at each location on the grid.

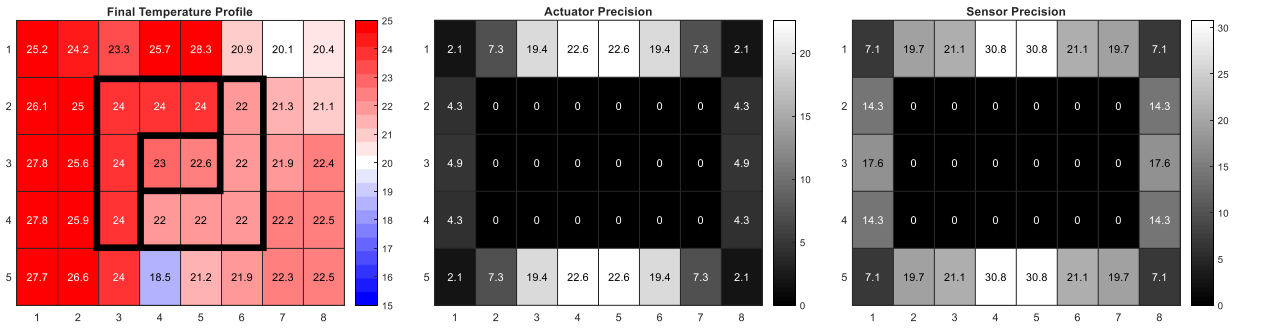

Figure 4: The final heat profile, actuator precision, and sensor precision values obtained using the developed design framework when actuators and sensors were placed along the wall.

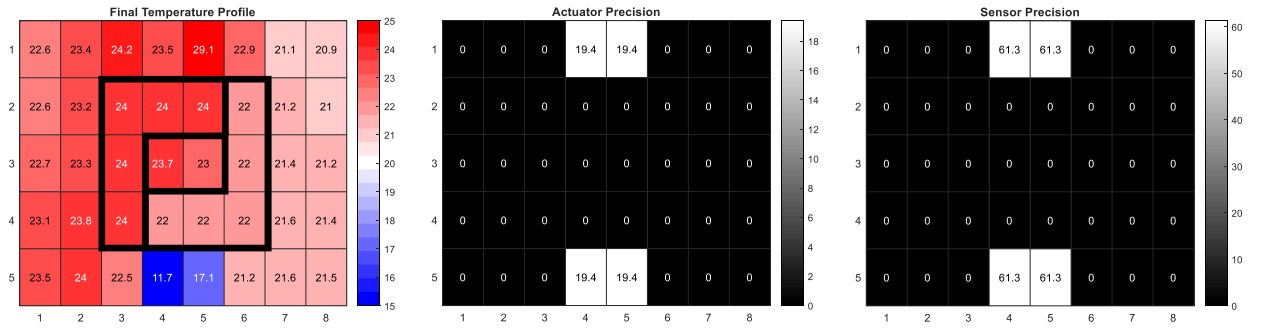

Figure 5: The final heat profile, actuator precision, and sensor precision obtained using the developed design framework when actuators and sensors were placed along the wall.

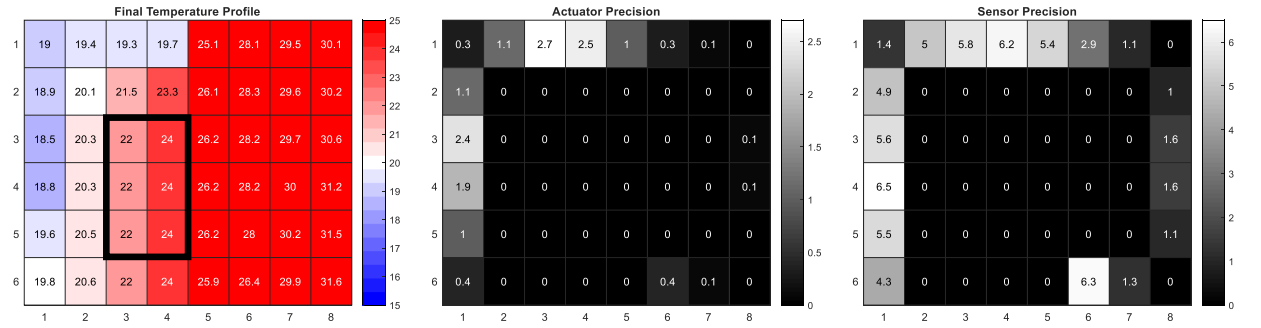

Figure 6: The final heat profile, actuator precision, and sensor precision values obtained using the developed design framework when actuators and sensors were placed at the wall.

ary grid points, achieving 22 and 24 $^{\circ}C$, respectively. As evident in Figure 4(middle) and (right), sensors and ac-

https://doi.org/10.26868/25222708.2023.1423

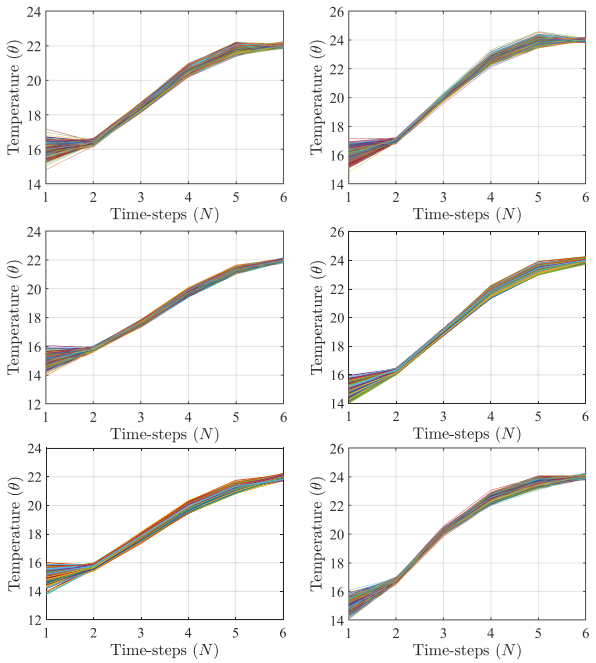

Figure 7: The temperature evolution profile for the selected grid points. The plots show the evolution of the 1000 trajectories with a given initial uncertainty in the temperature and reduce the final uncertainty/variation in the temperature.

tuators are exclusively placed at the grid points along the wall.

In this case, the highest precision is observed in the middle of the north and south walls. These results are sensible given the 5X8 grid configuration, which is elongated in the horizontal direction. This configuration highlights the effectiveness of the constrained placement strategy in controlling the temperature profile within the meeting room.

Building upon these results, Figure 5 showcases the performance of the optimal control law when selecting the top 4 sensors and actuators. By leveraging this reduced set of instruments, the optimal control law can successfully regulate the desired temperatures within the bounding black boxes. This demonstrates the potential of the proposed methodology in achieving efficient temperature control while minimizing the number of required sensors and actuators.

Asymmetric Profile

Figure 2 (Right) illustrates the initial profile for an office where the meeting table has an asymmetric profile with respect to the room. The room size has been changed to 12X16 ft (6X8 grids), and the initial temperature profile varies in different areas of the room, which is often the case in spaces with limited sensing and actuation capabilities. In this scenario, we again assume that sensors and actuators can only be placed alongside the walls, with an additional constraint that they must maintain a minimum distance of two grids from the table to allow room for maneuverability around the table.

The results in Figure 6 demonstrate successful control to achieve the desired profile. It is important to note that the highest precision is required closest to the table, with sensor precision higher on the grid on the south wall, which is not required for actuation. This result highlights the effectiveness of the constrained and asymmetric placement strategy in controlling the temperature profile within the meeting room.

Finally, Figure 7 displays the temperature evolution profile for the selected grid points. The plots depict the evolution of 1000 trajectories, with a given initial uncertainty in temperature, and illustrate a reduction in the final uncertainty/variation in temperature. This reduction is an artifact of the optimization formulation.

It is important to note that the shrinking of covariance may be more desirable for certain grids than others, and this preference can be accounted for in the problem formulation. By considering these variations in desirability, the optimization process can be further refined to achieve more targeted and efficient temperature control within the meeting room.

Conclusion

This paper addresses the co-design of the controller and the optimal placement of actuators and sensors, as well as their precision values, by formulating it as a convex optimization problem. The proposed approach successfully balances the observability and controllability of the system, considering both collocated and distributed sensors/actuators, while adhering to constraints on their total number and associated costs.

The jointly optimized active control law effectively minimizes energy consumption while actively rejecting disturbances from external temperature changes, solar radiation, and imperfect actuators/sensors to achieve the desired temperature profile. The results reveal the efficacy of the sensor/actuator selection algorithm while providing performance bounds on the achievable temperature range.

For future research directions, the proposed methodology can be extended to integrate with existing legacy control systems, ensuring a seamless transition and enhanced performance in real-world applications. Maintaining a focus on occupant comfort, the framework can also be adapted to address other types of building systems or even extended to non-building domains where optimal sensor and actuator placement is crucial for efficient control. These extensions will further demonstrate the versatility and potential impact of the proposed approach in various fields and applications.

References

Arnesano, M., G. Revel, and F. Seri (2016). A tool for the optimal sensor placement to optimize temperature monitoring in large sports spaces. *Automation in Construction 68*, 223–234.

Bae, Y., S. Bhattacharya, B. Cui, S. Lee, Y. Li, L. Zhang, P. Im, V. Adetola, D. Vrabie, M. Leach, and T. Kuruganti (2021). Sensor impacts on building and hvac

controls: A critical review for building energy performance. *Advances in Applied Energy 4*, 100068.

Borggaard, J., J. A. Burns, A. Surana, and L. Zietsman (2009). Control, estimation and optimization of energy efficient buildings. In *2009 American Control Conference*, pp. 837–841.

Burns, J. A., J. Borggaard, E. Cliff, and L. Zietsman (2012). An optimal control approach to sensor/actuator placement for optimal control of high performance buildings. *International High Performance Buildings Conference. 76*.

Chen, X. and X. Li (2016). Virtual temperature measurement for smart buildings via bayesian model fusion. In *2016 IEEE International Symposium on Circuits and Systems (ISCAS)*, pp. 950–953. IEEE.

Georges, D. (1995). The use of observability and controllability gramians or functions for optimal sensor and actuator location in finite-dimensional systems. In *Proceedings of 1995 34th ieee conference on decision and control*, Volume 4, pp. 3319–3324. IEEE.

Goyal, R., M. Majji, and R. E. Skelton (2021a). Integrating structure, information architecture and control design: Application to tensegrity systems. *Mechanical Systems and Signal Processing 161*, 107913.

Goyal, R., M. Majji, and R. E. Skelton (2021b). Optimal actuator/sensor precision for covariance steering with soft convex constraints on state and control. In *2021 American Control Conference (ACC)*, pp. 5015–5022. IEEE.

Goyal, R. and R. E. Skelton (2019). Joint optimization of plant, controller, and sensor/actuator design. In *2019 American Control Conference (ACC)*, pp. 1507–1512.

Kim, J. W., Y. K. Jeong, and I. W. Lee (2012). Automatic sensor arrangement system for building energy and environmental management. *Energy Procedia 14*, 265–270. 2011 2nd International Conference on Advances in Energy Engineering (ICAEE).

Li, F., M. C. de Oliveira, and R. E. Skelton (2008, March). Integrating Information Architecture and Control or Estimation Design. *SICE Journal of Control, Measurement, and System Integration Vol.1*(No.2).

Qiao, H., X. Han, S. Nabi, and C. R. Laughman (2019). Coupled simulation of a room air-conditioner with cfd models for indoor environment. In *Proceedings of the 13th International Modelica Conference, Regensburg, Germany, March 4–6, 2019*, Number 157. Linköping University Electronic Press.

Tian, W., Y. Fu, Q. Wang, T. A. Sevilla, and W. Zuo (2018). Optimization on thermostat location in an office room using the coupled simulation platform in modelica buildings library: a pilot study. In *The 4th International Conference on Building Energy and Environment (COBEE2018)*.

Tran, D. H., M. H. Nazari, A. Sadeghi-Mobarakeh, and H. Mohsenian-Rad (2019). Smart building design: a framework for optimal placement of smart sensors and actuators. In *2019 IEEE Power & Energy Society Innovative Smart Grid Technologies Conference (ISGT)*, pp. 1–5.

Vaidya, U., R. Rajaram, and S. Dasgupta (2012). Actuator and sensor placement in linear advection pde with building system application. *Journal of Mathematical Analysis and Applications 394*(1), 213–224.

Yoganathan, D., S. Kondepudi, B. Kalluri, and S. Manthapuri (2018). Optimal sensor placement strategy for office buildings using clustering algorithms. *Energy and Buildings 158*, 1206–1225.

Zuo, W., M. Wetter, W. Tian, D. Li, M. Jin, and Q. Chen (2016). Coupling indoor airflow, hvac, control and building envelope heat transfer in the modelica buildings library. *Journal of Building Performance Simulation 9*(4), 366–381.